



New PEO-IAA-Inspired Anti-Auxins: Synthesis, Biological Activity, and Possible Application in Hemp (*Cannabis Sativa* L.) Micropropagation

Asta Žukauskaitė¹ · Iñigo Saiz-Fernández² · Kristýna Bielešová¹ · Monika Iškauskienė³ · Chao Zhang⁴ · Iva Smýkalová⁵ · Karolina Dzedulionytė³ · Martin F. Kubeš^{4,6} · Michaela Sedlářová⁷ · Barbora Pařízková⁴ · Iva Pavlović⁴ · Thomas Vain^{8,9} · Ivan Petřík⁴ · Vida Malinauskienė³ · Algirdas Šačkus³ · Miroslav Strnad⁴ · Stéphanie Robert⁸ · Richard Napier⁶ · Ondřej Novák⁴ · Karel Doležal^{1,4}

Received: 3 February 2023 / Accepted: 2 May 2023
© The Author(s) 2023

Abstract

Auxins play an important role in plant physiology and are involved in numerous aspects of plant development, such as cell division, elongation and differentiation, fruit development, and phototropic response. In addition, through their antagonistic interaction with cytokinins, auxins play a key role in the regulation of root growth and apical dominance. Thanks to this capacity to determine plant architecture, natural and synthetic auxins have been successfully employed to obtain more economically advantageous plants. The crosstalk between auxins and cytokinins determines plant development and thus is of particular importance in the field of plant micropropagation, where the ratios between these two phytohormones need to be tightly controlled to achieve proper rooting and shoot generation. Previously reported anti-auxin PEO-IAA, which blocks auxin signalling through binding to TIR1 receptor and inhibiting the expression of auxin-responsive genes, has been successfully used to facilitate hemp micropropagation. Herein, we report a set of new PEO-IAA-inspired anti-auxins capable of antagonizing auxin responses *in vivo*. The capacity of these compounds to bind to the TIR1 receptor was confirmed *in vitro* by SPR analysis. Using DESI-MSI analysis, we evaluated the uptake and distribution of the compounds at the whole plant level. Finally, we characterized the effect of the compounds on the organogenesis of hemp explants, where they showed to be able to improve beneficial morphological traits, such as the balanced growth of all the produced shoots and enhanced bud proliferation.

Keywords Anti-auxin · *Arabidopsis thaliana* · Indole-3-acetic acid (IAA) · Multiple shoot culture · DESI-MSI analysis · SPR analysis

Introduction

Phytohormones are naturally occurring compounds capable of modulating plant developmental, physiological, and metabolic processes, even at low concentrations (Fonseca et al. 2014; Hemelíková et al. 2021). The application of phytohormones to manipulate plant development started in the 1930s, when ethylene and the related compound acetylene

were used to alter flowering and fruit formation in pineapple (Bartholomew 2014). Since then, the exogenous application of phytohormones to plants has become a staple in agricultural and horticultural practices (Rademacher 2015). A better understanding of plant hormones and the structural requirements essential for their biological activity has allowed the creation of synthetic analogues, which have found use not only in agriculture, as growth promoters and herbicides, but also in plant science as tools to study different biological processes (Rigal et al. 2014; Jiang and Asami 2018).

Auxins, amongst which indole-3-acetic acid (IAA) is the most abundant one, were the first class of phytohormones to be discovered and had been postulated to regulate plant growth a century before their chemical identity was revealed (Enders and Strader 2015). Auxins are key regulators of

Handling Editor: Serena Varotto.

Asta Žukauskaitė, Iñigo Saiz-Fernández, Kristýna Bielešová, Monika Iškauskienė, Chao Zhang, and Iva Smýkalová contributed equally to this work.

Extended author information available on the last page of the article

many aspects of plant development, including cell division, elongation and differentiation, fruit development, and organ photo- and gravitropism (Enders and Strader 2015). Canonical auxin signalling is dependent on nuclear Transport Inhibitor Response 1/Auxin Signalling F-box protein (TIR1/AFB) auxin receptors, which are capable of both binding the auxin and acting as F-box ubiquitin ligases mediating ubiquitination and protein degradation of Aux/IAA transcriptional repressors. These repressors interact and modulate the activity of several Auxin Response Factors (ARFs), the latter being able to recognize auxin response elements (AREs) in the promoter region of auxin-controlled genes with variable specificity and affinity (Gallei et al. 2020). Additionally, very rapid cellular non-transcriptional responses to auxin, such as the triggering of changes in plasma membrane potential, have been known for decades (Dubey et al. 2021). Since recently, processes that were believed to be regulated through the canonical TIR1/AFB pathway, such as the regulation of root growth, are now being reconsidered, as such responses are too fast to involve transcription and protein expression, suggesting that an unknown non-transcriptional branch of TIR1/AFB signalling exists (Friml et al. 2022). Selective auxin agonists, such as RubNeddins (RNs) (Vain et al. 2019), and antagonists, such as 4-(2,4-dimethylphenyl)-2-(1*H*-indol-3-yl)-4-oxobutanoic acid (auxinole) and 2-(1*H*-indol-3-yl)-4-oxo-4-phenylbutanoic acid (PEO-IAA) (Hayashi et al. 2012), can be used to study and regulate various plant growth and development processes. These anti-auxins have been suggested to bind to TIR1, block the formation of the TIR1-IAA-Aux/IAA complex, and thus inhibit the expression of auxin-responsive genes (Hayashi et al. 2012).

Thanks to the capacity to determine plant architecture, auxins, anti-auxins, and cytokinins, on their own or in combination, have been successfully employed to yield plants with delayed senescence and improved grain yield, drought resistance, seed set, flowering, etc. (Shi et al. 2014; Tamaki et al. 2015; Koprna et al. 2016; Liang et al. 2020; Klos et al. 2022). Moreover, through their antagonistic interaction auxins and cytokinins play an essential role in the regulation of root and shoot growth (Aloni et al. 2006; Umehara et al. 2008; Kurepa and Smalle 2022), which is of particular importance in the field of plant micropropagation, where the ratio between these two groups of phytohormones needs to be tightly controlled in order to achieve proper shoot growth and rooting (Holmes et al. 2021).

Hemp (*Cannabis sativa* L.), a traditional multi-purpose crop which over the centuries has found applications in many areas, such as pharmaceutical, textile, paper and construction industries, animal feeding, or biofuel production (Crini et al. 2020), is one of many species that could benefit from advancements in micropropagation techniques. Even though large-scale hemp cultivation has

traditionally been done through seed cultivation, using heavily mechanized agricultural practices similar to other grain crops (Monthony et al. 2021b), for pharmaceutical uses clonal methods for plant propagation tend to be favoured, as they allow the production of genetically and phenotypically uniform, pathogen and disease-free plants with consistent growth rates (Crini et al. 2020; Monthony et al. 2021b). Unfortunately, hemp clonal propagation in vitro has been proven to be particularly challenging due to the strong apical dominance (Smýkalová et al. 2019; Dreger and Szalata 2021) and the tendency to form callus (Movahedi et al. 2016), which is associated with bud organogenic recalcitrance (Monthony et al. 2021a). Achieving direct regeneration in hemp is problematic (Galán-Ávila et al. 2020), often resulting in a reduced regenerative responsiveness in vitro. This is usually attributed to the significant genetic variability within each variety, which is further exacerbated by diversity in the ploidy status and occasional polyploidisation event (Mansouri and Bagheri 2017; Crawford et al. 2021; Balant et al. 2022), as well as to the variability in the representation of female and male plants; even though most individuals are dioecious, monoecious cultivars also exist (Balant et al. 2022).

During the last couple of years, several synthetic auxin and cytokinin derivatives such as *meta*-topolin (mT) (Lata et al. 2016), thidiazuron (TDZ) (Lata et al. 2009; Piuanno et al. 2019; Dreger and Szalata 2021), 6-benzylaminopurine (BAP) and 1-naphthalene acetic acid (NAA) (Burgel et al. 2020) have been tested to better control the growth of new tissues, highlighting the potential use of novel synthetic phytohormone derivatives in hemp clonal propagation. Moreover, we have previously demonstrated that the weak anti-auxin PEO-IAA, applied in combination with the cytokinin *N*-benzyl-9-(tetrahydro-2*H*-pyran-2-yl) adenine (BAP9THP), is able to efficiently suppress the apical dominance of newly forming shoots in hemp. Such co-treatment resulted in a balanced multiple shoot culture which could be reliably rooted (Smýkalová et al. 2019). Therefore, the use of molecules with an anti-auxin character to suppress auxin activity and manipulate cytokinin to auxin ratio in explants, thus facilitating bud organogenesis or embryogenesis, appears to be promising.

In this study, we aimed to further expand the library of available anti-auxins that could be used both for improving plant micropropagation as well as a tool in fundamental plant research. Thus, we synthesized several 4-([1,1'-biphenyl]-4-yl)-2-(1*H*-indol-3-yl)-4-oxobutanoic acid derivatives, evaluated their anti-auxin activity in various auxin bioassays in vivo, studied their effect on root and hypocotyl growth on the model plant *Arabidopsis thaliana*, and tested their possible use in hemp explant clonal propagation.

Materials and Methods

Reagents and General Synthetic Methods

The reagents and solvents were purchased from commercial suppliers and used without further purification. The microwave irradiation-assisted reactions were performed in CEM Discover SP microwave reactor; the reactions were carried out in 10 mL glass vials that were sealed with silicone/PTFE caps. Reaction progress was monitored by thin-layer chromatography (TLC) on aluminium plates coated with silica gel 60 F254 (Merck, USA) and the components were visualized by UV light (254 and 365 nm) and staining solutions (vanillin or potassium permanganate). The purification of the products was performed by column chromatography on silica gel (40–63 micron Davisil LC60 A, Grace Davison, UK). ^1H (500 MHz) and ^{13}C (125 MHz) NMR spectra were recorded in DMSO- d_6 or acetone- d_6 as solvents at room temperature on a Jeol ECA-500 spectrometer equipped with a 5 mm Royal probe. Complete assignment of the ^1H and ^{13}C NMR resonances was achieved using a combination of standard NMR spectroscopic techniques, including heteronuclear single quantum coherence (HSQC) and heteronuclear multiple bond correlation (HMBC) experiments. Asterisk (*) indicates tentative assignment of solvent-overlapping signals based on ^1H , ^{13}C -HMQC experiment. High-resolution mass spectrometry (HRMS) spectra of test compounds were recorded with a micrOTOF-Q III Bruker spectrometer in electron spray ionization mode. The LC–MS analyses were performed on an ACQUITY UPLC® H-Class system combined with UPLC® PDA detector and a single-quadrupole mass spectrometer QDa™ (Waters, Manchester, UK) as previously described (Bieleszová et al. 2019).

Synthesis of (*E*)-4-(4-Bromophenyl)-4-Oxobut-2-Enoic Acid 2

To a solution of maleic anhydride (490 mg, 5 mmol) in dichloromethane (40 mL), aluminium chloride (1350 mg, 10 mmol) was added portion-wise followed by bromobenzene (523 μL , 5 mmol). The resulting solution was stirred at room temperature for 4 h. Subsequently, reaction mixture was quenched with 1N HCl (50 mL) and extracted with ethyl acetate (3 \times 30 mL). The combined organic phases were washed with saturated ammonium chloride solution and brine, dried over anhydrous sodium sulphate, filtered, and evaporated under reduced pressure. The crude product was used in the next step without any additional purification.

Yield 99%, yellow solid, $R_f=0.29$ (ethyl acetate/methanol 1/0.1). ^1H NMR (500 MHz, DMSO- d_6): δ 6.68 (d,

$J=15.6$ Hz, 1H, CH), 7.76–7.80 (m, 2H, 2 \times CH), 7.84 (d, $J=15.5$ Hz, 1H, CH), 7.94–7.98 (m, 2H, 2 \times CH), 10.22 (s, 1H, COOH). ^{13}C NMR (125 MHz, DMSO- d_6) δ 128.3 (C), 130.9 (Ph 2 \times CH), 132.2 (Ph 2 \times CH), 133.3 (CH), 135.2 (C), 135.9 (CH), 166.3 (COOH), 188.9 (C=O). LC–MS (ESI, pos. mode) m/z (%): 255/257 (M + H $^+$, 96).

Synthesis of 4-(4-Bromophenyl)-2-(1*H*-Indol-3-yl)-4-Oxobutanoic Acid 3

A mixture of (*E*)-4-(4-bromophenyl)-4-oxobut-2-enoic acid 2 (1000 mg, 3.92 mmol) and indole (505 mg, 4.31 mmol) was heated at 80 °C in toluene (31 mL) for 8 h. Upon completion, resulting reaction mixture was concentrated to approximately 1/3 volume, diluted with petroleum ether, and then cooled. The formed precipitate was filtered off and recrystallized from a mixture of toluene and petroleum ether to obtain 4-(4-bromophenyl)-2-(1*H*-indol-3-yl)-4-oxobutanoic acid 3 which was further purified by column chromatography.

Yield 81%, beige solid. $R_f=0.77$ (ethyl acetate/methanol 1/0.1). ^1H NMR (500 MHz, acetone- d_6): δ 3.35 (dd, $J=18.1$, 2.3 Hz, 1H, CH(H)), 3.99–4.13 (m, 1H, CH(H)), 4.46–4.56 (m, 1H, CH), 6.98–7.12 (m, 2H, Ind 5,6-H), 7.30–7.41 (m, 2H, Ind 2,7-H), 7.64–7.77 (m, 3H, Ph 3,5-H; Ind 4-H), 7.99 (d, $J=7.4$ Hz, 2H, Ph 2,6-H), 10.22 (br s, 1H, NH). ^{13}C NMR (125 MHz, acetone- d_6): δ 38.6 (CH), 42.4 (CH $_2$), 112.3 (Ind C-7), 113.5 (Ind C-3), 119.8 (Ind C-5), 120.0 (Ind C-4), 122.4 (Ind C-6), 123.8 (Ind C-2), 127.5 (Ind C-3a), 128.3 (Ph C-4), 130.8 (Ph C-2,6), 132.7 (Ph C-3,5), 136.8 (Ph C-1), 137.7 (Ind C-7a), 175.1 (COOH), 198.0 (C=O). LC–MS (ESI, pos. mode) m/z (%): 372/374 (M + H $^+$, 100).

General Procedure for the Synthesis of 4-[(1,1'-Biphenyl)-4-yl]-2-(1*H*-Indol-3-yl)-4-Oxobutanoic Acids 4a-d

To a solution of 4-(4-bromophenyl)-2-(1*H*-indol-3-yl)-4-oxobutanoic acid 3 (261 mg, 0.7 mmol) in a mixture of ethanol (4.2 mL) and water (1.4 mL), appropriate phenylboronic acid (1.05 mmol), caesium carbonate (456 mg, 1.4 mmol), and palladium(II) acetate (16 mg, 0.07 mmol) were added under argon atmosphere. The mixture was stirred at 100 °C under microwave irradiation (100 W, 300 Pa) for 30 min. Upon completion, the reaction mixture was cooled to room temperature and filtered through a pad of Celite and the filter cake was washed with ethyl acetate (20 mL). The residue was diluted with water (20 mL) and extracted with ethyl acetate (3 \times 25 mL). The combined organic layers were washed with water (10 mL) and brine (10 mL), dried over anhydrous sodium sulphate, filtered, and then evaporated

under reduced pressure. The crude was purified by column chromatography.

Synthesis of 4-[(1,1'-Biphenyl)-4-yl]-2-(1*H*-Indol-3-yl)-4-Oxobutanoic Acid **4a**—BP-IAA

4-[(1,1'-Biphenyl)-4-yl]-2-(1*H*-indol-3-yl)-4-oxobutanoic acid **4a** was prepared in accordance with general procedure from 4-(4-bromophenyl)-2-(1*H*-indol-3-yl)-4-oxobutanoic acid **3** (261 mg, 0.7 mmol) and phenylboronic acid (128 mg, 1.05 mmol). Yield 77%, pale yellow crystals. $R_f=0.30$ (petroleum ether/ethyl acetate/methanol 1/2/0.05). ^1H NMR (500 MHz, acetone- d_6): δ 3.43 (dd, $J=18.0$, 3.8 Hz, 1H, *CH*(H)), 4.17 (dd, $J=18.0$, 10.6 Hz, 1H, *CH*(H)), 4.58—4.62 (m, 1H, CH), 7.04—7.09 (m, 1H, Ind 5-H), 7.11—7.16 (m, 1H, Ind 6-H), 7.38—7.44 (m, 3H, Ind 2,7-H; CPh 4-H), 7.47—7.52 (m, 2H, CPh 3,5-H), 7.71—7.75 (m, 2H, CPh 2,6-H), 7.78—7.83 (m, 3H, C(O)Ph 3,5-H; Ind 4-H), 8.15—8.18 (m, 2H, C(O)Ph 2,6-H), 10.27 (br s, 1H, NH). ^{13}C NMR (125 MHz, acetone- d_6): δ 38.6 (CH), 42.5 (CH₂), 112.3 (Ind C-7), 113.6 (Ind C-3), 119.8 (Ind C-5), 120.0 (Ind C-4), 122.4 (Ind C-6), 123.8 (Ind C-2), 127.5 (Ind C-3a), 127.9 (C(O)Ph C-3,5), 128.0 (CPh C-2,6), 129.1 (CPh C-4), 129.6 (C(O)Ph C-2,6), 129.9 (CPh C-3,5), 136.6 (C(O)Ph C-1), 137.7 (Ind C-7a), 140.6 (CPh C-1), 146.2 (C(O)Ph C-4), 175.2 (COOH), 198.3 (C=O). HRMS (ESI TOF) for C₂₄H₁₉NNaO₃⁺ ([M + Na]⁺): calcd 392.1257, found 392.1258.

Synthesis of 2-(1*H*-Indol-3-yl)-4-[2'-Methoxy-(1,1'-Biphenyl)-4-yl]-4-Oxobutanoic Acid **4b**—2MBP-IAA

2-(1*H*-Indol-3-yl)-4-[2'-methoxy-(1,1'-biphenyl)-4-yl]-4-oxobutanoic acid **4b** was prepared in accordance with general procedure from 4-(4-bromophenyl)-2-(1*H*-indol-3-yl)-4-oxobutanoic acid **3** (261 mg, 0.7 mmol) and 2-methoxyphenylboronic acid (160 mg, 1.05 mmol). Yield 79%, pale yellow solid. $R_f=0.30$ (petroleum ether/ethyl acetate/methanol 1/2/0.05). ^1H NMR (500 MHz, DMSO- d_6): δ 3.36—3.39* (m, 1H, *CH*(H)), 3.78 (s, 3H, OCH₃), 4.03—4.12 (m, 1H, *CH*(H)), 4.37 (dd, $J=10.7$, 3.7 Hz, 1H, CH), 6.99—7.17 (m, 4H, CPh 3,5-H; Ind 5,6-H), 7.33—7.43 (m, 4H, CPh 4,6-H; Ind 2,7-H), 7.63 (d, $J=8.4$ Hz, 2H, C(O)Ph 3,5-H), 7.70 (d, $J=7.9$ Hz, 1H, Ind 4-H), 8.07 (d, $J=8.4$ Hz, 2H, C(O)Ph 2,6-H), 11.04 (s, 1H, NH), 12.19 (s, 1H, OH). ^{13}C NMR (125 MHz, DMSO- d_6): δ 37.7 (CH), 41.1 (CH₂), 55.6 (OCH₃), 111.5 (Ind C-7), 111.9 (CPh C-3), 112.0 (Ind C-3), 118.6 (Ind C-5), 119.1 (Ind C-4), 120.9 (CPh C-5), 121.2 (Ind C-6), 123.3 (Ind C-2), 126.3 (Ind C-3a), 127.8 (C(O)Ph C-2,6), 128.7 (CPh C-1), 129.6 (C(O)Ph C-3,5), 129.8 (CPh C-4), 130.4 (CPh C-6), 134.8 (C(O)Ph C-1), 136.3 (Ind C-7a), 143.1 (C(O)Ph C-4), 156.17 (CPh

C-2), 174.8 (COOH), 198.0 (C=O). HRMS (ESI TOF) for C₂₅H₂₁NNaO₄⁺ ([M + Na]⁺): calcd 422.1363, found 422.1362.

Synthesis of 2-(1*H*-Indol-3-yl)-4-[3'-Methoxy-(1,1'-Biphenyl)-4-yl]-4-Oxobutanoic Acid **4c**—3MBP-IAA

2-(1*H*-Indol-3-yl)-4-[3'-methoxy-(1,1'-biphenyl)-4-yl]-4-oxobutanoic acid **4c** was prepared in accordance with general procedure from 4-(4-bromophenyl)-2-(1*H*-indol-3-yl)-4-oxobutanoic acid **3** (261 mg, 0.7 mmol) and 3-methoxyphenylboronic acid (160 mg, 1.05 mmol). Yield 81%, pale yellow solid. $R_f=0.27$ (petroleum ether/ethyl acetate/methanol 1/2/0.05). ^1H NMR (500 MHz, DMSO- d_6): δ 3.37—3.41* (m, 1H, *CH*(H)), 3.84 (s, 3H, OCH₃), 4.08 (dd, $J=18.1$, 10.7 Hz, 1H, *CH*(H)), 4.36 (dd, $J=10.6$, 3.8 Hz, 1H, CH), 6.98—7.04 (m, 2H, CPh 4-H; Ind 5-H), 7.06—7.13 (m, 1H, Ind 6-H), 7.26—7.45 (m, 5H, CPh 2,5,6-H; Ind 2,7-H), 7.70 (d, $J=7.9$ Hz, 1H, Ind 4-H), 7.84 (d, $J=8.2$ Hz, 2H, C(O)Ph 3,5-H), 8.11 (d, $J=8.3$ Hz, 2H, C(O)Ph 2,6-H), and 11.05 (s, 1H, NH), 12.21 (s, 1H, OH). ^{13}C NMR (125 MHz, DMSO- d_6): δ 37.7 (CH), 41.2 (CH₂), 55.2 (OCH₃), 111.5 (Ind C-7), 111.9 (Ind C-3), 112.5 (CPh C-2), 114.0 (CPh C-4), 118.6 (Ind C-5), 119.1 (Ind C-4), 119.3 (CPh C-6), 121.2 (Ind C-6), 123.3 (Ind C-2), 126.3 (Ind C-3a), 127.1 (C(O)Ph C-3,5), 128.7 (C(O)Ph C-2,6), 130.2 (CPh C-5), 135.4 (C(O)Ph C-1), 136.3 (Ind C-7a), 140.4 (CPh C-1), 144.5 (C(O)Ph C-4), 159.8 (CPh C-3), 174.8 (COOH), and 198.0 (C=O). HRMS (ESI TOF) for C₂₅H₂₁NNaO₄⁺ ([M + Na]⁺): calcd 422.1363, found 422.1363.

Synthesis of 2-(1*H*-Indol-3-yl)-4-[4'-Methoxy-(1,1'-Biphenyl)-4-yl]-4-Oxobutanoic Acid **4d**—4MBP-IAA

2-(1*H*-Indol-3-yl)-4-[4'-methoxy-(1,1'-biphenyl)-4-yl]-4-oxobutanoic acid **4d** was prepared in accordance with general procedure from 4-(4-bromophenyl)-2-(1*H*-indol-3-yl)-4-oxobutanoic acid **3** (261 mg, 0.7 mmol) and 4-methoxyphenylboronic acid (160 mg, 1.05 mmol). Yield 73%, yellow solid. $R_f=0.27$ (petroleum ether/ethyl acetate/methanol 1/2/0.05). ^1H NMR (500 MHz, DMSO- d_6): δ 3.31—3.34* (m, 1H, *CH*(H)), 3.81 (s, 3H, OCH₃), 4.07 (dd, $J=18.1$, 10.7 Hz, 1H, *CH*(H)), 4.32—4.39 (m, 1H, CH), 6.98—7.13 (m, 4H, CPh 3,5-H; Ind 5,6-H), 7.33—7.39 (m, 2H, Ind 2,7-H), 7.67—7.75 (m, 3H, CPh 2,6-H; Ind 4-H), 7.79 (d, $J=8.3$ Hz, 2H, C(O)Ph 3,5-H), 8.09 (d, $J=8.4$ Hz, 2H, C(O)Ph 2,6-H), 11.04 (s, 1H, NH), 12.19 (s, 1H, OH). ^{13}C NMR (125 MHz, DMSO- d_6): δ 37.7 (CH), 41.1 (CH₂), 55.3 (OCH₃), 111.5 (Ind C-7), 112.0 (Ind C-3), 114.6 (CPh C-3,5), 118.6 (Ind C-5), 119.1 (Ind C-4), 121.2 (Ind C-6), 123.3 (Ind C-2), 126.2 (C(O)Ph C-3,5), 126.3 (Ind C-3a),

128.2 (CPh C-2,6), 128.8 (C(O)Ph C-2,6), 131.1 (CPh C-1), 134.6 (C(O)Ph C-1), 136.3 (Ind C-7a), 144.3 (C(O)Ph C-4), 159.7 (CPh C-4), 174.8 (COOH), 197.9 (C=O). HRMS (ESI TOF) for $C_{25}H_{21}NNaO_4^+$ ($[M + Na]^+$): calcd 422.1363, found 422.1362.

SPR Analysis

Surface plasmon resonance (SPR) experiments were done in accordance to previously described protocols (Lee et al. 2014). TIR1 was expressed in insect cell culture using a recombinant baculovirus. The construct contained sequences for three affinity tags, namely 6 His, green fluorescent protein (GFP), and FLAG. Protein purified using the His tag was used for SPR assays by passing it over a streptavidin chip loaded with biotinylated IAA7 degron peptide in the presence of IAA and test compounds.

The SPR buffer was Hepes-buffered saline with 10 mM Hepes, 3 mM EDTA, 150 mM NaCl and 0.05% Tween-20. Compounds were premixed prior to testing with the protein to a final 50 μ M concentration. Binding experiments were run at a flow rate of 30 μ l min^{-1} using 2 min of injection time and 4 min of dissociation time. Data from a control channel (a mutated IAA7 peptide) and from a buffer-only run supplemented with DMSO (final 1%) were subtracted from each sensorgram following the standard double-reference subtraction protocol.

DESI-MSI and DESI-MS/MSI Analyses

Arabidopsis thaliana wild-type ecotype Col-0 seeds were sterilized with 70% EtOH with 0.1% Tween-20 solution for 10 min (2 \times) and rinsed with 96% EtOH for 10 min. After 2 days of stratification (4 °C in dark), seeds germinated on sterile 1/2 MS medium (2.2 g/L Murashige and Skoog medium, 1% sucrose and 0.7% agar—all from Duchefa Biochemie, the Netherlands, 0.5 g/L MES PUFFERAN from Carl Roth GmbH, Germany, pH 5.6) in long-day light conditions (22 °C/20 °C, 16 h light/8 h dark, 100 μ mol $\text{m}^{-2} \text{s}^{-1}$). Ten-day-old seedlings were transferred to horizontally divide heterogeneous media containing 1/2 MS (1.5% agar) medium supplemented with 0.05% dimethyl sulfoxide (DMSO) and 0.25% acetonitrile (ACN) (top half of the plate) or 0.05% DMSO, 0.25% ACN, and 10 μ M of the tested compounds (bottom half of the plate). Plates were covered with aluminium foil and kept in a growth chamber with long-day light conditions (22 °C/20 °C, 16 h light/8 h dark, 100 μ mol $\text{m}^{-2} \text{s}^{-1}$) in a vertical position for 24 h. Around 50–70 mm-long plants were freshly collected together with untreated control samples for Desorption Electrospray Ionization—Mass Spectrometry Imaging (DESI-MSI) and Liquid Chromatography—Tandem Mass Spectrometry (LC-MS/MS) analyses. The whole plant was rapidly washed

in ultrapure water for 10 s to remove surface medium and mounted on Superfrost glass slides (Thermo Fisher Scientific, Waltham, MA, USA) using non-conductive double-sided tape (Plano GmbH, Wetzlar, Germany) and stored in – 80 °C freezer. Sample slides were rapidly dried in a vacuum desiccator (Merck), scanned, and then subjected to DESI-MSI acquisition. The acquired spectra were recalibrated using the exact mass of palmitic acid (m/z 255.2324) and processed into an imzml format at the HDImaging (Waters). Subsequent analysis was performed using the msi-Quant (Uppsala, Sweden), where the data were processed for low-intensity removal, total ion count (TIC) normalization, peak alignment, and ion intensity map establishment. Deprotonated ions, representing compounds uptaken into the plants, were binning within the 0.0001 Da mass range of their theoretical masses after calibration. Target compounds BP-IAA, 2MBP-IAA, 3MBP-IAA, 4MBP-IAA, PEO-IAA, and auxinole assigned as deprotonated masses m/z 368.1292, 398.1398, 398.1398, 398.1398, 292.0979, and 320.1292 and were used to establish the ion intensity maps and following statistical analysis.

To validate the results of targeted compounds detected in the DESI-MSI analysis, in situ MS/MS analysis was performed using 2–3 mm of primary root tips from treated plants. Precursor ions of BP-IAA (m/z 368.1292), its methoxy derivatives (m/z 398.1398), PEO-IAA (m/z 292.0979), and auxinole (m/z 320.1292) were scanned at 60 μ m spatial resolution and fragmented using 5 eV collision energy. Additionally, peaks with the molecular mass assigned to the indole ring, ions after the loss of an indole ring, and decarboxylated ions of BP-IAA, its methoxy derivatives, PEO-IAA, and auxinole were also identified and assigned.

DR5::GUS Assay

Arabidopsis thaliana seeds expressing pDR5::GUS (Ulmasov et al. 1997) in a Col-0 background were sterilized with 70% EtOH with 0.1% Tween-20 solution for 10 min (2 \times) and rinsed with 96% EtOH for 10 min. After 2 days of stratification (4 °C in dark), seeds germinated on sterile 1/2 MS medium (2.2 g/L Murashige and Skoog medium, 1% sucrose, and 0.7% agar—all from Duchefa Biochemie, the Netherlands, 0.5 g/L MES PUFFERAN from Carl Roth GmbH, Germany, pH 5.6) in long-day light conditions (22 °C/20 °C, 16 h light/8 h dark, 100 μ mol $\text{m}^{-2} \text{s}^{-1}$). Five-day-old seedlings were incubated at room temperature in 24-well plates containing 1 mL of 1/2 MS liquid media supplemented with auxin derivatives in a final concentration of 20 μ M, with 0.5% DMSO as a mock and 2 μ M IAA as a positive control. The compounds were applied for 5 h treatment. Additionally, seedlings of the *Arabidopsis thaliana* transgenic pDR5::GUS reporter line were treated with auxin derivatives in defined concentrations (1, 5 μ M) in the

presence of 2 μM IAA for 5 h. Seedlings were then incubated in the presence of 500 μL of GUS staining solution at 37 $^{\circ}\text{C}$ in the dark for 35 min. To stop the staining reaction, seedlings were transferred to 500 μL of 70% ethanol and kept overnight. Clearing of the roots was done with HCG-2 solution (120 g chloral hydrate, 90 mL water, 30 mL glycerol) (Ma et al. 2020). GUS expression was evaluated using an inverted light microscope (Olympus IX51) with transmission light mode and phase contrast.

GUS staining solution

Na phosphate buffer, pH 7.0: 4.7 g of $\text{NaH}_2\text{PO}_4 \cdot \text{H}_2\text{O}$ and 9.6 g of $\text{Na}_2\text{HPO}_4 \cdot 2 \text{H}_2\text{O}$ from Merck were dissolved in 500 mL of distilled water to give a 0.2 M stock solution. 50 mL of Na phosphate buffer was supplemented with 0.08 g $\text{K}_3[\text{Fe}(\text{CN})_6]$ from Merck, 0.12 g $\text{K}_4[\text{Fe}(\text{CN})_6]$ from Lachema n.p., the Czech Republic, 50 μL 0.1% Triton from Koch-Light Laboratories, England, and 50 mg of X-Gluc from AppliChem GmbH, Germany dissolved in 500 μL of DMSO.

35S::DII-VENUS Assay

Arabidopsis thaliana seeds expressing p35S::DII-VENUS (Brunoud et al. 2012) in a Col-0 background were sterilized with 70% EtOH with 0.1% Tween-20 solution for 10 min (2 \times) and rinsed with 96% EtOH for 10 min. After 2 days of stratification (4 $^{\circ}\text{C}$ in dark), seeds germinated on sterile $\frac{1}{2}$ MS medium (2.2 g/L Murashige and Skoog medium, 1% sucrose, and 0.7% agar—all from Duchefa Biochemie, the Netherlands, 0.5 g/L MES PUFFERAN from Carl Roth GmbH, Germany, pH 5.6) in long-day light conditions (22 $^{\circ}\text{C}/20$ $^{\circ}\text{C}$, 16 h light/8 h dark, 100 $\mu\text{mol m}^{-2} \text{s}^{-1}$). Five-day-old seedlings were treated in liquid $\frac{1}{2}$ MS medium in the presence of BP-IAA compounds, auxinole and PEO-IAA (5 μM in 0.5% DMSO) or DMSO as a control for 1 h. The seedlings were then transferred to a glass slide with a drop of untreated medium and confocal images were taken using a Zeiss LSM 900 confocal microscope (Carl Zeiss, Germany) with a 10 \times objective and resolution of 1024 \times 1024 px. VENUS fluorescent protein was excited at 488 nm. At least 30 plants belonging to three independent biological replicates were measured.

Root Growth Assay

Arabidopsis thaliana wild-type ecotype Col-0 seeds were sterilized with 70% EtOH with 0.1% Tween-20 solution for 10 min (2 \times) and rinsed with 96% EtOH for 10 min. After 2 days of stratification (4 $^{\circ}\text{C}$ in dark), seeds germinated on sterile $\frac{1}{2}$ MS medium (2.2 g/L Murashige and Skoog medium, 1% sucrose, and 0.7% agar—all from Duchefa

Biochemie, the Netherlands, 0.5 g/L MES PUFFERAN from Carl Roth GmbH, Germany, pH 5.6) supplemented with 0.3% DMSO as a mock or 0.5 μM IAA as a positive control and tested compounds in defined concentrations (1, 5, 10, 20 μM) with or without the presence of 0.5 μM IAA for 5 days in long-day light conditions (22 $^{\circ}\text{C}/20$ $^{\circ}\text{C}$, 16 h light/8 h dark, 100 $\mu\text{mol m}^{-2} \text{s}^{-1}$). Primary root length was measured using ImageJ software (<https://imagej.nih.gov/ij/>) and normalized to mock. At least 30 plants belonging to three independent biological replicates were measured.

Hypocotyl Elongation and Cytoskeletal Organization Assay

Arabidopsis thaliana MBD::GFP seeds (Marc et al. 1998) were sown in full MS (pH 5.7, 0.8% agar) and grown vertically in a growth chamber (22 $^{\circ}\text{C}/20$ $^{\circ}\text{C}$, 16 h light/8 h dark, 60 $\mu\text{mol m}^{-2} \text{s}^{-1}$ light intensity). Five days after sowing seedlings were transferred to a new media containing 5, 10, or 20 μM of either BP-IAA or auxinole, with and without co-treatment with 0.5 μM NAA (final DMSO concentration of 0.9%). All samples were examined 1 and 3 days after treatment using an Axio imager Z.1 platform equipped with LSM700 module (Carl Zeiss, Germany) using 40 \times oil objective, as previously described (Skalák et al. 2019). The light source included an argon–neon laser with wavelength 488 nm for GFP fluorescence and 639 nm for chlorophyll auto-fluorescence to avoid interference of the two fluorescence channels. Cell length and microtubule density (estimated as Mean Grey Intensity) were calculated using ImageJ software. The microtubule orientation and anisotropy of the microtubule array were also calculated on ImageJ, using the FibrilTool macro (Boudaoud et al. 2014). All parameters were calculated on at least 8 plants per treatment (at least 200 total cells per treatment), belonging to three independent biological replicates.

Micropropagation of Hemp (*Cannabis sativa* L.) from Nodal Segments

Monoecious hemp (*Cannabis sativa* L.) seeds, variety USO-31 (origin Ukraine), were obtained from the Czech Hemp Gene Bank (Agritec Ltd., the Czech Republic). Seeds were surface sterilized and germinated as described previously (Smýkalová et al. 2019) and nodal segments (i.e. the first node below the apex containing two meristems for two future shoots) were used as a type of an explant. For the experiment, 10 μM BAP9THP and 10 μM anti-auxin activity-possessing substances (BP-IAA, its methoxy derivatives, PEO-IAA, and auxinole) were added to the medium previously described (Smýkalová et al. 2019), which was supplemented with macro- and microelements (Murashige and Skoog 1962) and vitamins (Gamborg et al. 1968), 100 mg/L

myo-inositol, 40 mg/L adenine hemisulfate, 30 g/L sucrose, 5 g/L activated carbon, 5.5 g/L agar (Difco Bacto), and pH 5.8–6. Explants were cultured in a growth room at 21 ± 2 °C, light intensity $156 \mu\text{mol m}^{-2} \text{s}^{-1}$, 16 h photoperiod, and 60% relative humidity. Nineteen to twenty six explants per treatment, belonging to three (in case of BP-IAA) or four (in case of all other anti-auxins) biological replicates, were used. A selection of morphological parameters was recorded as either present or absent upon visual examination. Positively evaluated parameters for nodal segments: balanced growth of both shoots, proliferation of both buds, proliferation of more buds – i.e. more shoots, and proliferation of lateral buds at the base. Negatively evaluated parameters for nodal segments: formation of callus, long shoots, dominance of one shoot, and proliferation of one bud. The average number of shoots per explant was recorded. Data of positively and negatively evaluated parameters were processed with R 4.2.1 in environment of RStudio 2023.03.0 Build 386 (R Core Team 2022). Scripts were written using packages: stats 4.2.1, readxl 1.4.2, rstatix 0.7.2, ggplot2 3.4.2, and gridExtra 2.3. Chi-square test and respective *P*-values were computed by Monte Carlo simulation. Pairwise Fisher's test was used as a post hoc test with Bonferroni correction of calculated *P*-values. Significance level was set to $\alpha = 0.05$.

Results and Discussion

Synthesis of BP-IAA and its Methoxy Derivatives

The synthetic strategy for target compounds is depicted in Fig. 1. Firstly, (*E*)-4-(4-bromophenyl)-4-oxobut-2-enoic acid (**2**) (Drakulić et al. 2011) was readily prepared by Friedel–Crafts acylation of bromobenzene (**1**) with maleic acid anhydride in dichloromethane, using AlCl_3 as a Lewis acid

in accordance with previously reported procedure (Hayashi et al. 2012). In the next step, Michael addition of indole to (*E*)-4-(4-bromophenyl)-4-oxobut-2-enoic acid (**2**) in toluene at 80 °C afforded 4-(4-bromophenyl)-2-(1*H*-indol-3-yl)-4-oxobutanoic acid (**3**) (Sayed and Elhalim 1981) in 81% yield. Suzuki–Miyaura cross-coupling on auxin-like starting materials is typically done via a 3-step synthetic sequence, involving protection and deprotection of carboxylic acid group (Do-Thanh et al. 2016; Uchida et al. 2018; Torii et al. 2018). In this work, 4-(4-bromophenyl)-2-(1*H*-indol-3-yl)-4-oxobutanoic acid (**3**) was used in ligand-free Pd-catalysed Suzuki–Miyaura cross-coupling directly, without protection of carboxylic acid group as an ester. Namely, 4-(4-bromophenyl)-2-(1*H*-indol-3-yl)-4-oxobutanoic acid (**3**) was treated with various arylboronic acids in the presence of Cs_2CO_3 as a base and catalytic amount of $\text{Pd}(\text{OAc})_2$ in aqueous ethanol at 100 °C under microwave irradiation (Razmienė et al. 2021) furnishing products **4a–d** in 73–81% yield (Fig. 1). The latter were designated as BP-IAA and its methoxy analogues, 2MBP-IAA, 3MBP-IAA, and 4MBP-IAA, respectively (Fig. 2).

Determination of Biological Activity In Vitro by SPR Assay

First, using surface plasmon resonance (SPR) analysis (Lee et al. 2014), BP-IAA and its methoxy derivatives were tested for binding to auxin receptor TRANSPORT INHIBITOR RESPONSE 1 (TIR1) (Dharmasiri et al. 2005; Kepinski and Leyser 2005) and AUXIN/INDOLE-3-ACETIC ACID7 (IAA7) co-receptor complex (Villalobos et al. 2012). As anticipated, derivatization of the PEO-IAA core with aromatic substituents resulted in generation of compounds with anti-auxin activity. When mixed with purified TIR1, neither BP-IAA compounds, nor auxinole were able to support TIR1

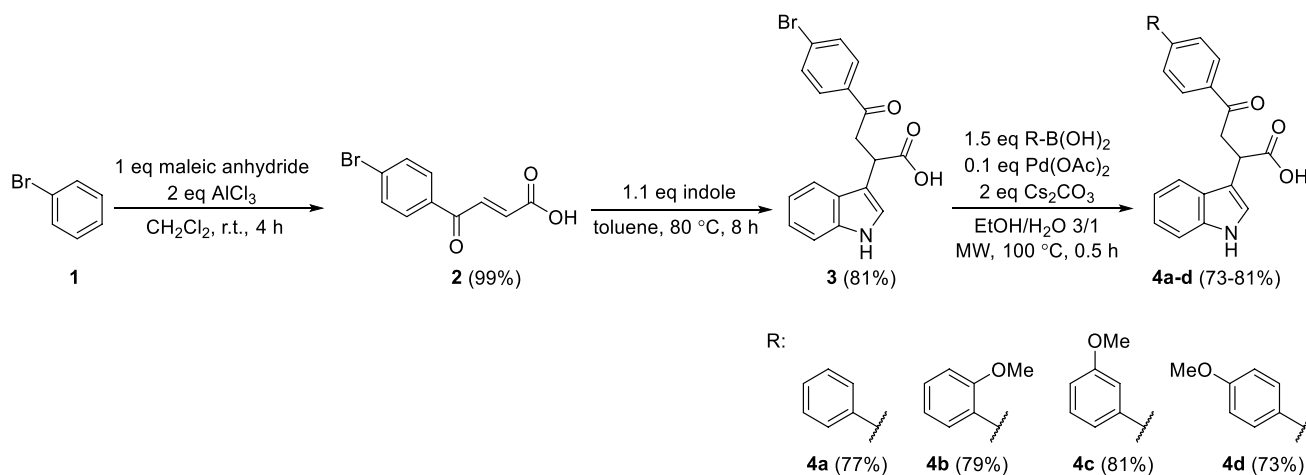


Fig. 1 Synthesis of BP-IAA compounds **4a–d**

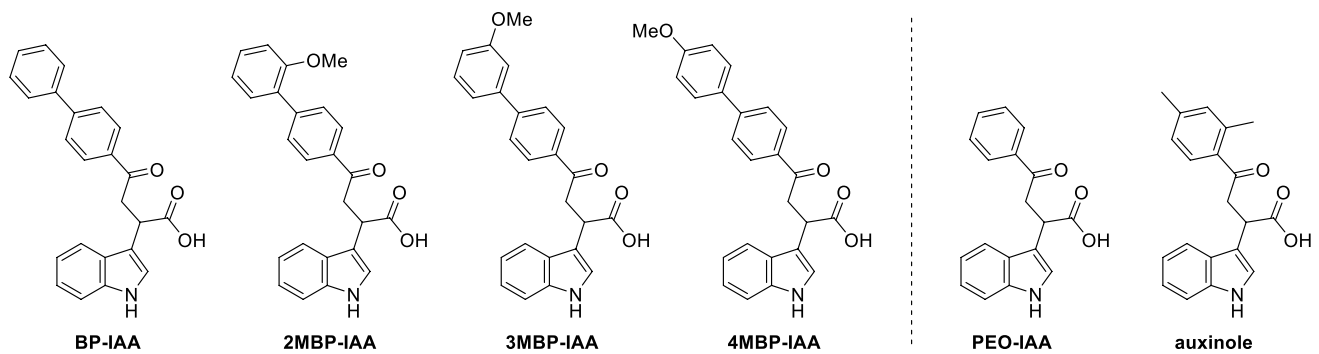


Fig. 2 Structures of PEO-IAA, auxinole, BP-IAA, and its methoxy derivatives

co-receptor assembly with IAA7 on the SPR chip even at 50 μM concentration (Supplementary Fig. S1). On the other hand, when co-treated with 5 μM IAA, BP-IAA compounds effectively inhibited TIR1 co-receptor assembly with IAA7 degen (Fig. 3A), by competing with IAA for its binding site, thus reducing the signal in a dose-dependent manner (Fig. 3B for BP-IAA).

Validation of Uptake in Planta

The uptake of lipophilic compounds into roots is considered to be fast; however, their transport to the upper plant parts is slow (Schriever and Lamshoeft 2020). Due to the bulky aromatic structures of BP-IAA compounds, confirmation of their uptake was needed prior to the *in vivo* experimentation. Desorption Electrospray Ionization-Mass Spectrometry Imaging (DESI-MSI) is emerging as a powerful tool for *in situ* identification and visualization of small molecules (Zhang et al. 2021). Therefore, ten-day-old *Arabidopsis thaliana* plants were transferred to $\frac{1}{2}$ MS media containing BP-IAA compounds and their presence in different plant tissues was visualized by desorption electrospray ionization—mass spectrometry (DESI-MS) and compared to the reference compounds PEO-IAA and auxinole (Fig. 4). In general, all six targeted compounds demonstrated high abundance in the primary root of treated plants, compared to the absence of peaks found in control plants (Fig. 4). The ions of BP-IAA and its methoxy derivatives were only detected in the mature root growing in the treated part of the medium, whereas the hypocotyl, root cap, elongation zone, and upper root in the non-treated part of the medium did not contain any aforementioned ions. In the case of the least lipophilic compound PEO-IAA (Supplementary Table S1), a high signal intensity level was observed not only in the mature regions but also in almost all imaging tissues, from the root cap to hypocotyl and epicotyl. The ions of auxinole were widely present in the primary root attached to the treated medium with robust signal intensities (Fig. 4).

To validate the results of targeted compounds detected in the DESI-MSI, *in situ* MS/MS analysis was performed using 2–3 mm of primary root tips from treated plants. Notably, the peak assigned as the indole ring was identified in all fragmentation spectra and displayed very similar distributions with precursor masses of targeted compounds in their ion intensity maps (Fig. 5). Peaks of decarboxylated ions were identified and assigned for all the compounds, whilst peaks representing ions after the loss of the indole ring were identified for all compounds except PEO-IAA. In summary, peaks predicted as fragmentation ions of targeted compounds matched previous records in the standard fragmentation spectra and their spatial distributions were compatible with the ion intensity maps established by precursor masses, which proved the presence of targeted compounds in the treated plants.

Determination of Biological Activity in *Arabidopsis* Roots

The anti-auxin activity of BP-IAA compounds predicted by the SPR analysis was confirmed *in vivo* employing *Arabidopsis* auxin-responsive reporter line pDR5::GUS. This line possesses a β -glucuronidase (GUS) reporter gene fused to the artificial canonical DR5 auxin-responsive promoter. The regulation of GUS expression responds to auxin levels, thus allowing the visualization of auxin maxima (Bai and DeMason 2008). Similarly to auxinole and PEO-IAA, BP-IAA compounds did not induce pDR5::GUS expression in *Arabidopsis* primary roots. On the other hand, likewise to auxinole, all BP-IAA compounds were able to overcome 2 μM IAA-induced GUS expression at 5 μM concentration, whilst the effect of PEO-IAA was milder (Fig. 6).

Additionally, the activity of BP-IAA compounds was further evaluated using DII-VENUS line, which expresses fluorescently labelled Aux/IAA auxin interaction DII domain (Brunoud et al. 2012). The DII domain is ubiquitinated and induces degradation of the protein in response to the auxin dose-dependent presence. The fluorescent signal is rapidly

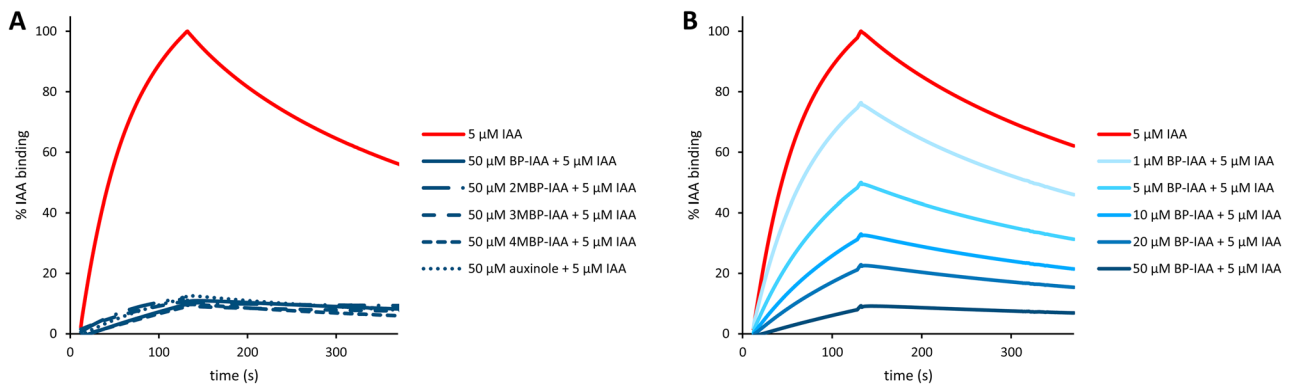


Fig. 3 SPR analysis of the antagonistic effect of BP-IAA and its methoxy derivatives on auxin-induced interaction between TIR1 protein and IAA7 degen peptide. The sensorgrams show association for 120 s followed by dissociation in buffer for 240 s. Results for IAA

(5 μM) on TIR1 protein alone (red) and **A** in co-treatment with BP-IAA, its methoxy derivatives, and auxinole (each at 50 μM) and **B** in co-treatment with BP-IAA in a concentration range (1, 5, 10, 20, 50 μM) (Color figure online)

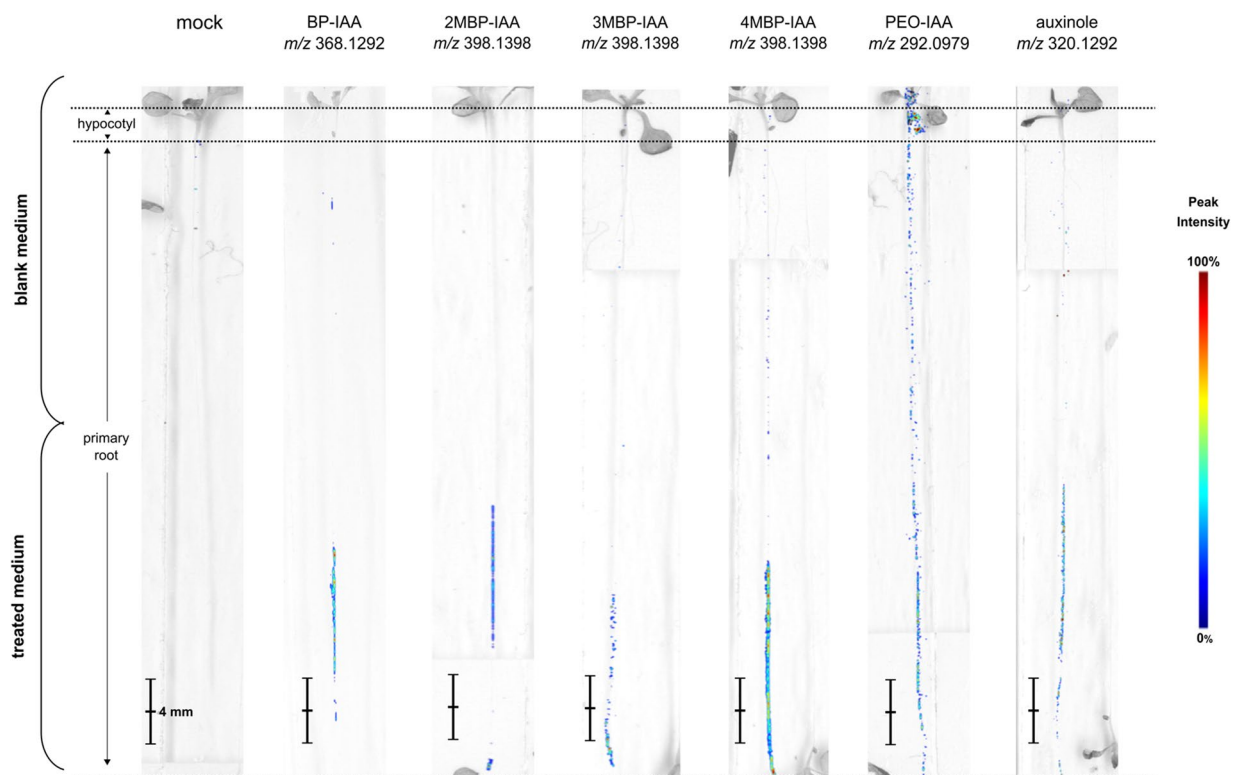


Fig. 4 DESI-MSI analysis revealing the different abundances of BP-IAA, 2MBP-IAA, 3MBP-IAA, 4MBP-IAA, PEO-IAA, and auxinole ions in the treated (each at 10 μM) *Arabidopsis* plant samples. Ion

intensity maps were established using RMS normalized peak intensities of targeted compounds. The signal intensity levels are displayed in the nearby scale bar

degraded in response to exogenously applied auxin, whilst it increases upon treatment with TIR1-IAA-Aux/IAA complex formation inhibitor auxinole (Hazak et al. 2014). In a similar manner to auxinole and PEO-IAA, BP-IAA compounds induced the accumulation of the DII-VENUS reporter protein by repressing the endogenous IAA activity, resulting in

an increase in the fluorescent signal in the elongation zone of *Arabidopsis* primary root (Fig. 7, Supplementary Fig. S2).

Arabidopsis roots react to the addition of auxin by extremely rapid root growth inhibition which gets restored once the auxin source is removed (Fendrych et al. 2018). Additionally, auxin-induced root growth inhibition can be

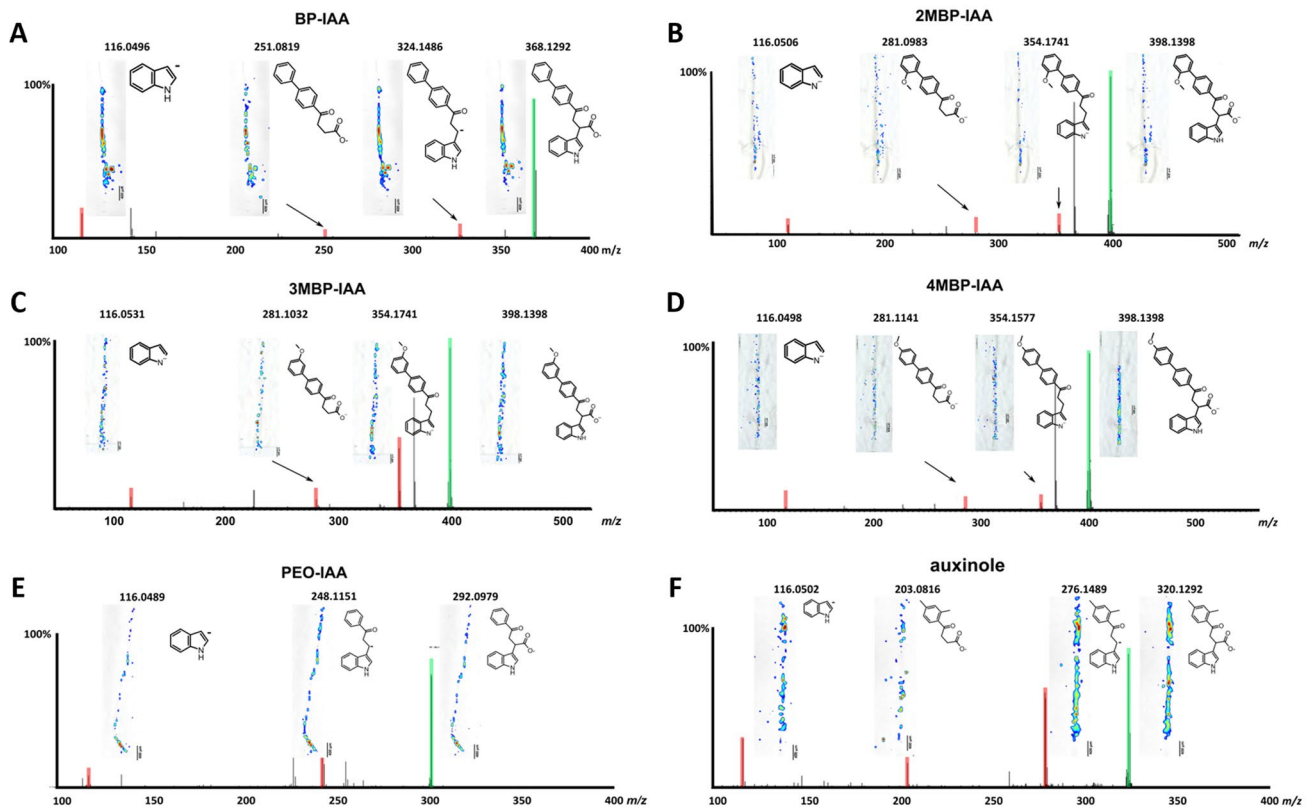


Fig. 5 DESI-MS/MSI analysis of targeted compounds (BP-IAA, its methoxy derivatives, PEO-IAA, and auxinole) precursor ions, major fragmentation ions, and their distribution patterns acquired from treated *Arabidopsis* primary root tip. The molecular formulas of the

identified fragments are also shown. Selected precursor masses of targeted compounds are marked in green. Identified fragmentation ions of target compounds using 5 eV collision energy are marked in red (Color figure online)

reverted by co-treatment with the auxin antagonist auxinole (Hayashi et al. 2012) or several other anti-auxin activity-possessing molecules (Bielezová et al. 2019). On the other hand, other known anti-auxins, such as PEO-IAA, BH-IAA, or PCIB, are not able to even partially revert auxin-induced root growth inhibition (Oono et al. 2003; Hayashi et al. 2012). As anticipated, at high concentrations BP-IAA derivatives slightly reduced primary root growth of *Arabidopsis* plants (Fig. 8A), which is a typical feature of anti-auxins (Oono et al. 2003; Hayashi et al. 2012). However, despite the observed anti-auxin effect in SPR assay, analogously to PEO-IAA and PCIB, BP-IAA compounds were not able to revert 0.5 μM IAA-induced root growth inhibition to the same extent as auxinole (Fig. 8B). This could suggest that BP-IAA compounds are probably not capable of antagonizing TIR1-independent auxin responses, such as the auxin-binding protein 1-transmembrane kinase 1 (ABP1-TMK1)-dependant auxin signalling pathway, which has been shown to modulate the activation of plasma membrane H^+ -ATPases, cell wall acidification, and cell expansion, amongst other processes (Lin et al. 2021; Friml et al. 2022).

Effect of BP-IAA on Hypocotyl Elongation and Cytoskeletal Organization

In the hypocotyl, auxins have been suggested to regulate cell expansion (Collett et al. 2000) and modulate microtubule orientation (Chen et al. 2014). It is generally assumed that there is a correlation between microtubule orientation and cell expansion, with transversal microtubule arrays usually being found in elongating cells (Baskin 2001; Chen et al. 2014); even though the causality between both parameters is still being discussed. The effect of the newly developed anti-auxins on microtubule orientation was analysed using *Arabidopsis thaliana* expressing a GFP-tagged binding domain of the microtubule associated protein 4 (MBD::GFP) (Marc et al. 1998). Five-day-old MBD::GFP plants treated with 0.5 μM NAA underwent a significant microtubule reorientation favouring longitudinally oriented fibres (60–90°) in detriment of transversal ones (0–30°), leading to a higher average microtubule angle (Table 1, Fig. 9, Supplementary Fig. S3). In agreement with the work of Chen et al. (Chen et al. 2014), *Arabidopsis* plants showed decreased hypocotyl cell elongation rate following NAA treatment (Table 1).

Fig. 6 The effect of BP-IAA derivatives on GUS expression in pDR5::GUS transgenic plants of *Arabidopsis thaliana*. Five-day-old seedlings were **A** kept untreated or treated with IAA (2 μ M), **B** BP-IAA compounds, auxinole or PEO-IAA (each at 20 μ M) for 5 h alone, or **C** co-treated with IAA (2 μ M) and with BP-IAA compounds, PEO-IAA, or auxinole (each at 1, 5 μ M) for 5 h. Figures were chosen as representatives from three independent biological repetitions

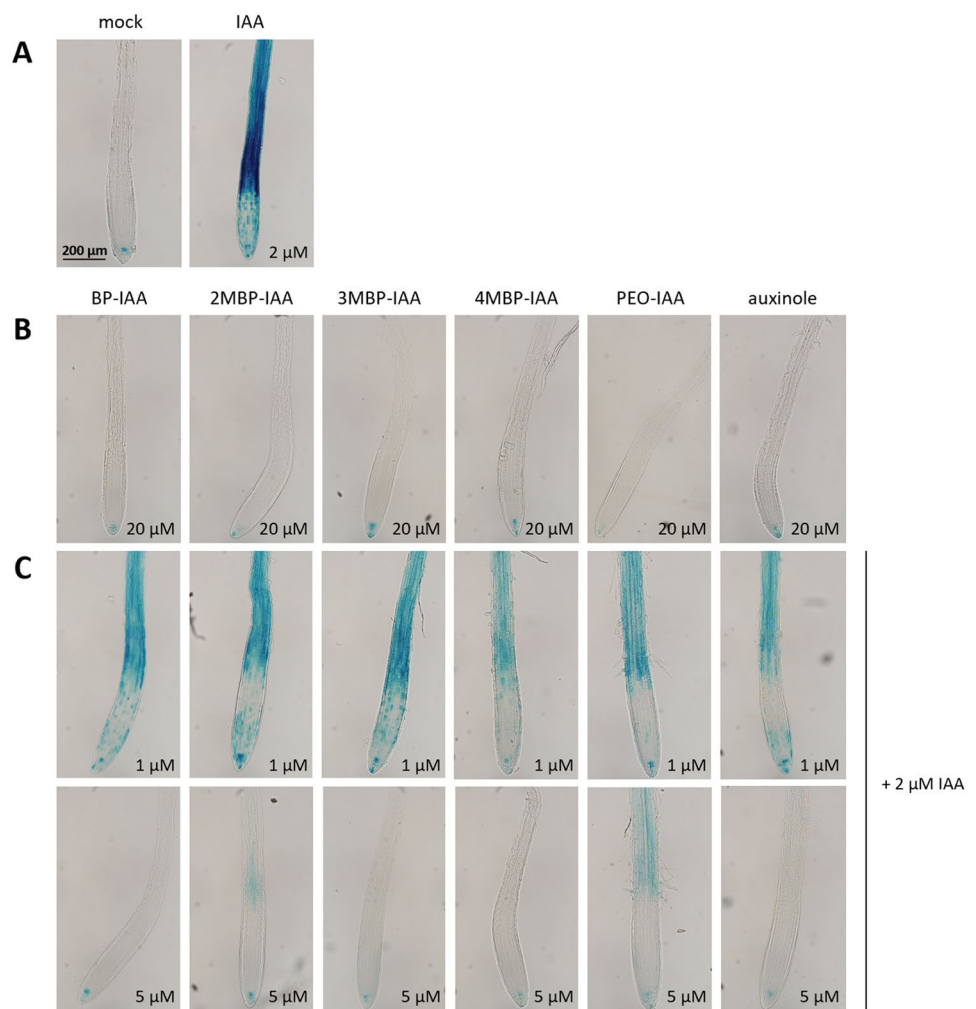
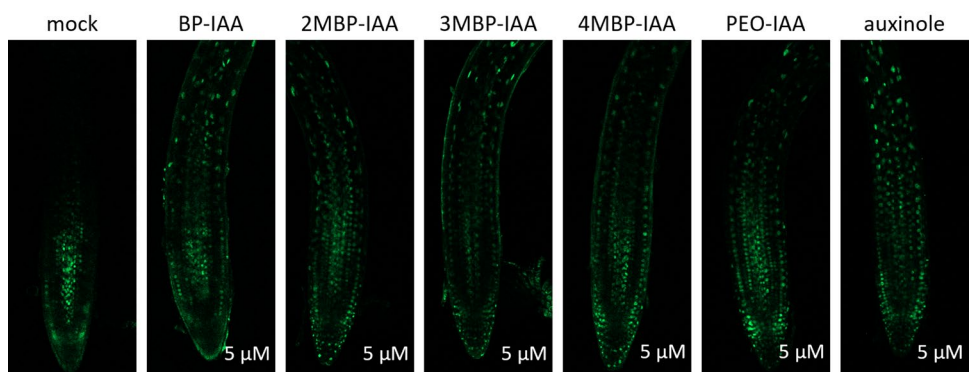


Fig. 7 The effect of BP-IAA compounds on DII-VENUS expression in p35S::DII-VENUS reporter line. Five-day-old seedlings were incubated with anti-auxins BP-IAA, its methoxy derivatives, PEO-IAA, or auxinole (each at 5 μ M) for 1 h. Fluorescent confocal images were chosen as representatives from three independent biological repetitions



Treatment with the auxinole had a similar effect as NAA on the microtubule orientation which, interestingly, was not dose dependent. Furthermore, treatment with 5 to 20 μ M of auxinole also decreased cell elongation rates in a fashion similar to NAA. This effect falls in line with the findings of Collett et al. (Collett et al. 2000), which suggest that auxin levels are already optimal in seedlings and any deviation from that concentration, either increase or decrease, results

in a decrease in cell elongation. On the contrary, treatment with BP-IAA had a less severe effect on cytoskeletal organization, but it affected it in a dose-dependent manner, with 5 μ M BP-IAA having no significant effect on microtubule orientation and 20 μ M BP-IAA showing an effect closer to that of NAA. This pattern was mirrored by the cell elongation rates, with 20 μ M resulting in decreased rates, whilst supply of 5 μ M BP-IAA showed no differences from controls

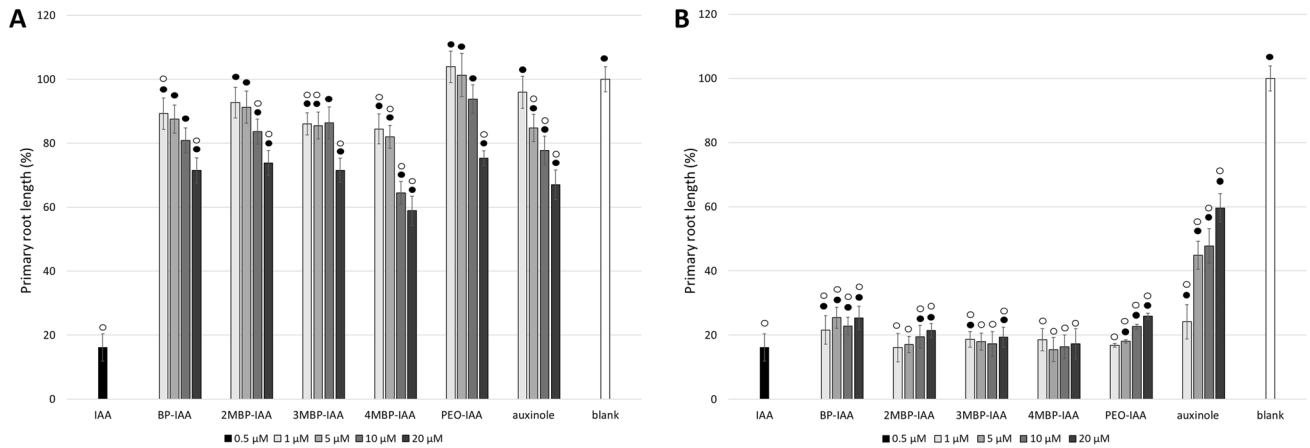


Fig. 8 The effect of BP-IAA derivatives on *Arabidopsis thaliana* (Col-0) primary root growth. The primary root length was quantified in five-day-old seedlings grown on BP-IAA compounds (each at 1, 5, 10, 20 μM) **A** in the absence or **B** presence of IAA (0.5 μM) and normalized to mock. IAA (0.5 μM), PEO-IAA, and auxinole (each at 1, 5, 10, 20 μM) were used as controls. Statistical analyses were per-

formed using the *t* test, values are means \pm S.E., and $n > 30$ from three independent replicates. White circles (○) indicate statistically significant differences ($P < 0.01$) compared to mock, whilst black circles (●) indicate statistically significant differences ($P < 0.01$) between the effect of BP-IAA compounds, PEO-IAA, and auxinole compared to 0.5 μM IAA treatment

Table 1 Microtubule angle (degrees), microtubule density and anisotropy of the microtubule array in five-day-old *Arabidopsis thaliana* MBD::GFP plants 1 day after treatment, and cell elongation rate ($\mu\text{m day}^{-1}$) between days 1 and 3 after treatment

Treatment	Cell elongation rate ($\mu\text{m day}^{-1}$)	Microtubule angle (degrees)	Microtubule density	Anisotropy
mock	10.6 \pm 0.6 ab	31 \pm 1 g	38 \pm 1 a	0.30 \pm 0.01 bc
NAA (0.5 μM)	1.9 \pm 0.7 e	45 \pm 2 abc	24 \pm 1 d	0.37 \pm 0.02 abc
BP-IAA (5 μM)	10.6 \pm 1.0 ab	34 \pm 2 efg	35 \pm 1 ab	0.29 \pm 0.01 c
BP-IAA (10 μM)	8.6 \pm 1.0 abc	37 \pm 2 defg	33 \pm 2 abc	0.33 \pm 0.02 abc
BP-IAA (20 μM)	6.3 \pm 0.9 bcd	45 \pm 2 abcd	33 \pm 2 abc	0.33 \pm 0.02 abc
BP-IAA (5 μM) + NAA (0.5 μM)	11.1 \pm 1.0 a	34 \pm 2 fg	36 \pm 1 a	0.34 \pm 0.01 abc
BP-IAA (10 μM) + NAA (0.5 μM)	9.2 \pm 0.8 ab	37 \pm 2 defg	35 \pm 2 ab	0.34 \pm 0.02 abc
BP-IAA (20 μM) + NAA (0.5 μM)	9.2 \pm 0.6 ab	37 \pm 3 cdefg	36 \pm 2 ab	0.35 \pm 0.02 abc
auxinole (5 μM)	2.8 \pm 1.0 de	51 \pm 1 a	24 \pm 1 d	0.33 \pm 0.02 abc
auxinole (10 μM)	4.2 \pm 1.0 cde	46 \pm 2 ab	27 \pm 1 cd	0.31 \pm 0.02 abc
auxinole (20 μM)	1.1 \pm 0.7 e	52 \pm 2 a	23 \pm 1 d	0.35 \pm 0.02 abc
auxinole (5 μM) + NAA (0.5 μM)	0.6 \pm 1.3 e	43 \pm 2 abcde	22 \pm 1 d	0.39 \pm 0.01 a
auxinole (10 μM) + NAA (0.5 μM)	1.6 \pm 1.1 e	40 \pm 2 bcdef	27 \pm 2 bcd	0.38 \pm 0.02 ab
auxinole (20 μM) + NAA (0.5 μM)	8.9 \pm 0.7 abc	32 \pm 2 cdefg	27 \pm 1 cd	0.35 \pm 0.01 abc

Values show mean \pm S.E.; $n \geq 8$ plants. Different letters indicate statistically significant differences between treatments according to Tukey's test ($P < 0.05$)

(Table 1). Co-treatment with auxinole started to counteract the effect of NAA in microtubule orientation and cell elongation rate at 10 μM , but only managed to completely revert to the values found in controls at a concentration of 20 μM (Table 1). On the contrary, co-treatment with BP-IAA showed a greater effect at counteracting NAA, as a concentration of 5 μM was enough to revert the effect of NAA and bring the average microtubule angle back to the values found

in controls (Table 1). Lastly, none of the treatments resulted in a decrease in the level of organization of the microtubule array (anisotropy) (Table 1).

When plants are subjected to certain stresses, such as salinity, low temperature, or hormonal and ROS unbalance, they usually undergo microtubule depolymerization and a consequent decrease in cytoskeleton density (Zhang et al. 2012; Fujita et al. 2013; Araniti et al. 2016). In this case,

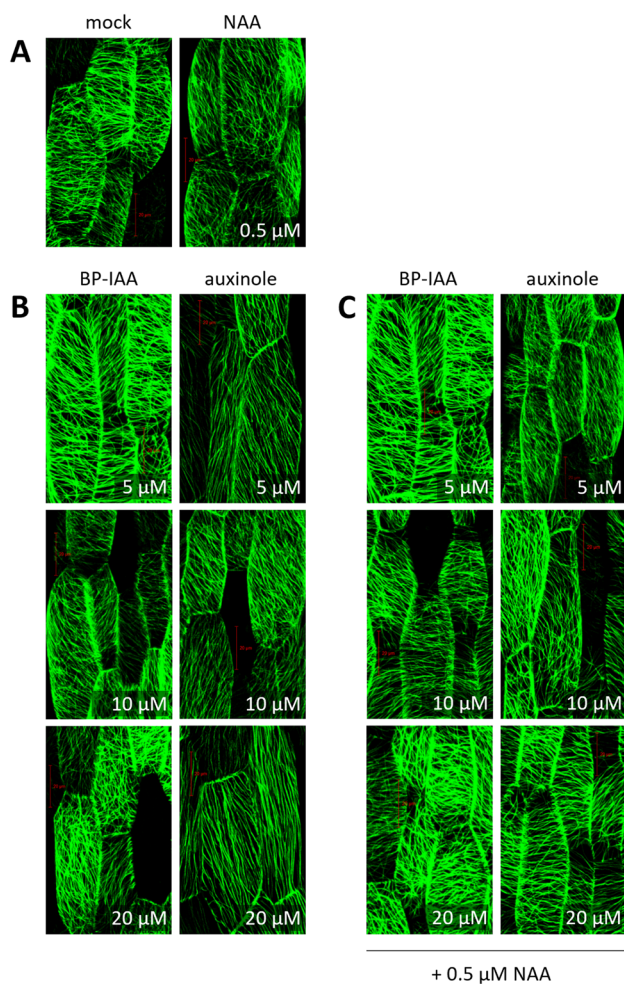


Fig. 9 The effect of BP-IAA derivatives on microtubule orientation in the hypocotyl of *Arabidopsis thaliana* MBD::GFP plants. Five-day-old seedlings were **A** kept untreated or treated with NAA (0.5 μ M), **B** treated with BP-IAA or auxinole (each at 5, 10, 20 μ M) for 1 day alone, or **C** co-treated with NAA (0.5 μ M). Figures were chosen as representatives from three independent biological repetitions

external NAA supply, in addition to inducing a microtubule reorientation, also decreased microtubule density (Table 1). Similarly, when added independently, both auxinole and

BP-IAA might have created stress, which decreased microtubule density, even though the effect was much more acute in the case of auxinole. However, the difference between auxinole and BP-IAA got accentuated when they were applied in co-treatment with NAA. In that context, no concentration of auxinole reverted the effect of NAA on microtubule density, whilst 5 μ M of BP-IAA was enough to bring the microtubule density back to the values found in controls. This highlights the contradiction between the effect of BP-IAA alone (where it shows a milder disruptive effect on cell growth and cytoskeletal organization than auxinole) and in combination with NAA (where it counteracts the effect of NAA at lower concentrations than auxinole), which deserves further investigation.

Application of BP-IAA Compounds in Hemp Micropropagation

In our previous work, we demonstrated that weak anti-auxin PEO-IAA can efficiently suppress apical dominance of newly forming shoots in hemp. Co-treatment with BAP-9THP and PEO-IAA gave a balanced multiple shoot culture for the formation of shoots which could be reliably rooted (Smýkalová et al. 2019). Having established PEO-IAA as a valuable component of hemp propagation medium, we further analysed if micropropagation of hemp could be further improved using BP-IAA compounds as a choice of anti-auxin.

The experiments were conducted on nodal segments of variety USO-31, using the newly prepared anti-auxins at 10 μ M concentration in combination with 10 μ M BAP9THP as a choice of a cytokinin. The previously described methodological procedure was used (Smýkalová et al. 2019) and a selection of positive and negative parameters was visually evaluated for each node and recorded as either present or absent (Fig. 10). In addition, the average number of shoots per explant was calculated.

The comparison of positive and negative morphological traits of explants after the application of anti-auxins in a medium intended for the induction of multiple shoot

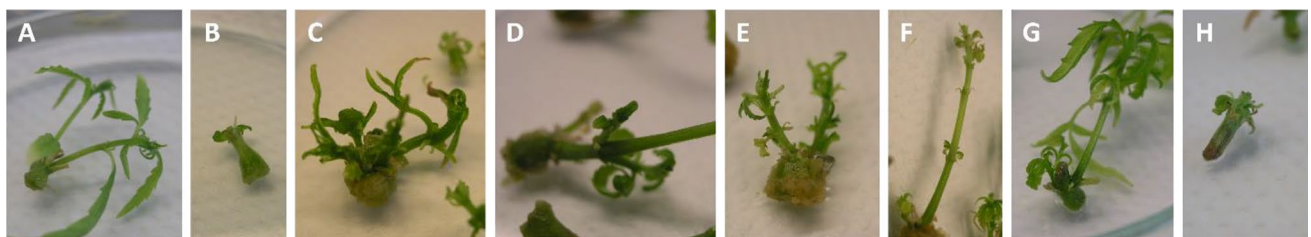


Fig. 10 Examples of positively **A–D** and negatively **E–H** evaluated parameters at nodes: balanced growth of both shoots (**A**), proliferation of both buds (**B**), proliferation of more buds/shoots (**C**), prolif-

eration of lateral buds at the base (**D**), callus (**E**), longer shoots (**F**), dominance of one shoot (**G**), and proliferation of one bud (**H**)

Table 2 Average number of shoots per node (mean ± SE) and percentage of hemp explants showing positively (white to blue scale) and negatively (white to red scale) evaluated morphological traits after

	BP-IAA	2MBP-IAA	3MBP-IAA	4MBP-IAA	PEO-IAA	auxinole
Shoots per node (mean ± SE)	1.89 ± 0.11 ab	1.57 ± 0.12 b	1.73 ± 0.10 ab	1.88 ± 0.07 ab	2.04 ± 0.07 a	1.84 ± 0.16 ab
Balanced growth of both shoots (%)	100	96.4	95.5	91.7	61.5	92.0
Proliferation of both buds (%)	83.3	71.4	72.7	87.5	88.5	60.0
Proliferation of more buds (%)	5.6	0	0	0	7.7	16.0
Proliferation of lateral buds (%)	0	0	0	0	69.2	68.0
Callus (%)	61.1	25.0	54.5	50.0	53.8	52.0
Long shoots (%)	5.6	3.6	27.3	20.8	38.5	16.0
Dominance of one shoot (%)	0	3.6	4.5	20.8	3.8	8.0
Proliferation of one bud (%)	16.7	14.3	27.3	16.7	3.8	16.0

application of 10 μM of BAP9THP and 10 μM of anti-auxins. Different letters indicate statistically significant differences between treatments according to Tukey's test ($P < 0.05$) (Color figure online)

culture (MSC) in hemp micropropagation culture is shown in Table 2, Supplementary Fig. S4 and Supplementary Table S2. After cutting off the shoot apex, the nodal segment contains two meristems for the proliferation of two shoots. Due to high auxin concentrations in hemp nodal segments, apical dominance of one of the two shoots and callus formation are commonly observed in MSC (Smýkalová et al. 2019; Dreger and Szalata 2021). In the present study, co-treatment with BAP9THP and BP-IAA derivatives suppressed the apical dominance, resulting in uniform development of both buds from one node and the reduction or prevention of callus formation on the basal part. Out of the four tested novel compounds, BP-IAA and 4MBP-IAA yielded the highest number of shoots per explant, which was comparable to that of auxinole and PEO-IAA. Moreover, in the case of BP-IAA, as well as the known anti-auxins auxinole and PEO-IAA, a slight increase in the percentage of explants that displayed proliferation of more buds was observed, which can enable easier multiplication of meristems. However, it should be noted that none of the BP-IAA compounds promoted the proliferation of lateral buds at the base that was observed with auxinole and PEO-IAA.

The application of 10 μM BP-IAA compounds yielded a low percentage of explants with long shoots or with dominance of only one shoot. The use of BP-IAA was particularly positive regarding dominance of one shoot, and it showed better results than PEO-IAA. On the contrary, PEO-IAA was the best option for keeping a low percentage of plants with only one developed bud. Lastly, the number of plants which developed callus was relatively high in case of all tested compounds, with 2MBP-IAA being the most potent to prevent callus formation.

Conclusion

In this work, we prepared a set of novel indolic compounds which are absorbed by *Arabidopsis thaliana* primary root and showed strong anti-auxin activity in SPR assay. Further testing of biological activity in vivo using *Arabidopsis* pDR5::GUS and p35S::DII-VENUS lines proved that BP-IAA and its methoxy derivatives overcome the effect of exogenous and endogenous auxin, respectively. BP-IAA was also shown to counteract the effect of exogenous auxins on *Arabidopsis* hypocotyl elongation, without any strong negative effect on its own. Lastly, we tested the use of BP-IAA and its methoxy derivatives in hemp micropropagation as a supplement for the establishment of multiple shoot cultures, where they improved positive morphological traits, such as the balanced growth of all the produced shoots and the proliferation of more than one bud, without negatively affecting the explants.

Supplementary Information The online version contains supplementary material available at <https://doi.org/10.1007/s00344-023-11031-x>.

Acknowledgements We would like to thank Prof. Jozef Šamaj (Department of Biotechnology, Faculty of Science, Palacký University Olomouc, Olomouc, Czech Republic) for kindly providing seeds of the *Arabidopsis thaliana* MDB::GFP transgenic line.

Author Contributions Conceptualization—AŽ, Methodology—AŽ, IS-F, CZ, IS, TV, SR, and RN. Investigation—AŽ, IS-F, KB, MI, CZ, IS, KDz, MFK, MSe, IPa, and BP. Formal analysis—AŽ, IS-F, KB, CZ, IS, KDz, MFK, IPe, VM, and AŠ. Visualization—AŽ, IS-F, and CZ. Data Curation—AŽ, IS-F, CZ, IS, and RN. Resources—AŽ, IS, MSt, SR, ON, KDo, and RN. Writing of the Original Draft—AŽ. Writing, Reviewing, and Editing of the manuscript—IS-F. All authors have read and agreed to the published version of the manuscript.

Funding Open access publishing supported by the National Technical Library in Prague. This work was supported by the Ministry of Education, Youth and Sports of the Czech Republic through the European Regional Development Fund-Project “Centre for Experimental Plant Biology” (CZ.02.1.01/0.0/0.0/16_019/0000738), by the Palacký University Olomouc Young Researcher Grant (JG_2020_002), by the Internal Grant Agency of Palacký University (IGA_PrF_2023_016), by the Ministry of Agriculture of the Czech Republic (MZE-RO1018), by the Horizon 2020 (H2020-MSCA-IF-2017–792329), by Vetenskapsrådet VR 2013–4632 and VINNOVA (to TV and SR), and The Knut and Alice Wallenberg Foundation ShapeSystems Grant 2012–050 (to SR). The authors acknowledge use of the Biacore T200 SPR instrument provided by the WISB Research Technology Facility within the School of Life Sciences, University of Warwick.

Declarations

Conflict of Interest On behalf of all authors, the corresponding authors state that there is no conflict of interest.

Open Access This article is licensed under a Creative Commons Attribution 4.0 International License, which permits use, sharing, adaptation, distribution and reproduction in any medium or format, as long as you give appropriate credit to the original author(s) and the source, provide a link to the Creative Commons licence, and indicate if changes were made. The images or other third party material in this article are included in the article's Creative Commons licence, unless indicated otherwise in a credit line to the material. If material is not included in the article's Creative Commons licence and your intended use is not permitted by statutory regulation or exceeds the permitted use, you will need to obtain permission directly from the copyright holder. To view a copy of this licence, visit <http://creativecommons.org/licenses/by/4.0/>.

References


- Aloni R, Aloni E, Langhans M, Ullrich CI (2006) Role of Cytokinin and Auxin in Shaping Root Architecture: Regulating Vascular Differentiation, Lateral Root Initiation, Root Apical Dominance and Root Gravitropism. *Ann Bot* 97:883–893. <https://doi.org/10.1093/aob/mcl027>
- Araniti F, Graña E, Krasuska U et al (2016) Loss of Gravitropism in Farnesene-Treated Arabidopsis Is Due to Microtubule Malformations Related to Hormonal and ROS Unbalance. *PLoS ONE*. <https://doi.org/10.1371/journal.pone.0160202>
- Bai F, DeMason DA (2008) Hormone interactions and regulation of PsPK2::GUS compared with DR5::GUS and PID::GUS in Arabidopsis thaliana. *Am J Bot* 95:133–145. <https://doi.org/10.3732/ajb.95.2.133>
- Balant M, Rodríguez González R, Garcia S et al (2022) Novel Insights into the Nature of Intraspecific Genome Size Diversity in Cannabis sativa L. *Plants* 11:2736. <https://doi.org/10.3390/plants11202736>
- Bartholomew DP (2014) History and perspectives on the role of ethylene in pineapple flowering. *Acta Hort* 1042:269–283
- Baskin TI (2001) On the alignment of cellulose microfibrils by cortical microtubules: A review and a model. *Protoplasma* 215:150–171. <https://doi.org/10.1007/BF01280311>
- Bieleszová K, Pařízková B, Kubeš M et al (2019) New fluorescently labeled auxins exhibit promising anti-auxin activity. *N Biotechnol* 48:44–52. <https://doi.org/10.1016/j.nbt.2018.06.003>
- Boudaoud A, Burian A, Borowska-Wykręt D et al (2014) FibrilTool, an ImageJ plug-in to quantify fibrillar structures in raw microscopy images. *Nat Protoc* 9:457–463. <https://doi.org/10.1038/nprot.2014.024>
- Brunoud G, Wells DM, Oliva M et al (2012) A novel sensor to map auxin response and distribution at high spatio-temporal resolution. *Nature* 482:103–106. <https://doi.org/10.1038/nature10791>
- Burgel L, Hartung J, Schibano D, Graeff-Hönninger S (2020) Impact of different phytohormones on morphology, yield and cannabinoid content of Cannabis sativa L. *Plants* 9:725. <https://doi.org/10.3390/plants9060725>
- Chen X, Grandont L, Li H et al (2014) Inhibition of cell expansion by rapid ABP1-mediated auxin effect on microtubules. *Nature* 516:90. <https://doi.org/10.1038/nature13889>
- Collett CE, Harberd NP, Leyser O (2000) Hormonal interactions in the control of Arabidopsis hypocotyl elongation. *Plant Physiol* 124:553–562. <https://doi.org/10.1104/PP.124.2.553>
- Crawford S, Rojas BM, Crawford E et al (2021) Characteristics of the diploid, triploid, and tetraploid versions of a cannabigerol-dominant F1 hybrid industrial hemp cultivar, cannabis sativa ‘stem cell CBG.’ *Genes (Basel)* 12:923. <https://doi.org/10.3390/genes12060923>
- Crini G, Lichtfouse E, Chanet G, Morin-Crini N (2020) Applications of hemp in textiles, paper industry, insulation and building materials, horticulture, animal nutrition, food and beverages, nutraceuticals, cosmetics and hygiene, medicine, agrochemistry, energy production and environment: a review. *Environ Chem Lett* 18:1451–1476. <https://doi.org/10.1007/s10311-020-01029-2>
- Dharmasiri N, Dharmasiri S, Estelle M (2005) The F-box protein TIR1 is an auxin receptor. *Nature* 435:441–445. <https://doi.org/10.1038/nature03543>
- Do-Thanh CL, Vargas JJ, Thomas JW et al (2016) Design, synthesis, and evaluation of novel auxin mimic herbicides. *J Agric Food Chem* 64:3533–3537. <https://doi.org/10.1021/acs.jafc.6b00675>
- Drakulić BJ, Stanojković TP, Žižak ŽS, Dabović MM (2011) Antiproliferative activity of aroylacrylic acids. Structure-activity study based on molecular interaction fields. *Eur J Med Chem* 46:3265–3273. <https://doi.org/10.1016/j.ejmech.2011.04.043>
- Dreger M, Szalata M (2021) The Effect of TIBA and NPA on Shoot Regeneration of Cannabis sativa L. Epicotyl Explants *Agronomy* 12:104. <https://doi.org/10.3390/agronomy12010104>
- Dubey SM, Serre NBC, Oulehlová D et al (2021) No time for transcription—rapid auxin responses in plants. *Cold Spring Harb Perspect Biol*. <https://doi.org/10.1101/cshperspect.a039891>
- Enders TA, Strader LC (2015) Auxin activity: past, present, and future. *Am J Bot* 102:180–196. <https://doi.org/10.3732/ajb.1400285>
- Fendrych M, Akhmanova M, Merrin J et al (2018) Rapid and reversible root growth inhibition by TIR1 auxin signalling. *Nat Plants*. <https://doi.org/10.1038/s41477-018-0190-1>
- Fonseca S, Rosado A, Vaughan-Hirsch J et al (2014) Molecular locks and keys: the role of small molecules in phytohormone research. *Front Plant Sci*. <https://doi.org/10.3389/fpls.2014.00709>
- Friml J, Gallei M, Gelová Z et al (2022) ABP1–TMK auxin perception for global phosphorylation and auxin canalization. *Nature* 609:575–581. <https://doi.org/10.1038/s41586-022-05187-x>
- Fujita S, Pytela J, Hotta T et al (2013) An atypical tubulin kinase mediates stress-induced microtubule depolymerization in Arabidopsis. *Curr Biol* 23:1969–1978. <https://doi.org/10.1016/J.CUB.2013.08.006>
- Galán-Ávila A, García-Fortea E, Prohens J, Herraiz FJ (2020) Development of a direct in vitro plant regeneration protocol from Cannabis sativa L. seedling explants: developmental morphology of shoot regeneration and ploidy level of regenerated plants. *Front Plant Sci*. <https://doi.org/10.3389/fpls.2020.00645>
- Gallei M, Luschnig C, Friml J (2020) Auxin signalling in growth: Schrödinger’s cat out of the bag. *Curr Opin Plant Biol* 53:43–49. <https://doi.org/10.1016/j.pbi.2019.10.003>

- Gamborg OL, Miller RA, Ojima K (1968) Nutrient requirements of suspension cultures of soybean root cells. *Exp Cell Res* 50:151–158. [https://doi.org/10.1016/0014-4827\(68\)90403-5](https://doi.org/10.1016/0014-4827(68)90403-5)
- Hayashi K, Neve J, Hirose M et al (2012) Rational design of an auxin antagonist of the SCF^{TIR1} auxin receptor complex. *ACS Chem Biol* 7:590–598. <https://doi.org/10.1021/cb200404c>
- Hazak O, Obolski U, Prat T et al (2014) Bimodal regulation of ICR1 levels generates self-organizing auxin distribution. *Proc Natl Acad Sci U S A* 111:E5471–E5479. <https://doi.org/10.1073/pnas.1413918111>
- Hemelíková N, Žukauskaitė A, Pospíšil T et al (2021) Caged phytohormones: from chemical inactivation to controlled physiological response. *J Agric Food Chem* 69:12111–12125. <https://doi.org/10.1021/acs.jafc.1c02018>
- Holmes JE, Lung S, Collyer D, Punja ZK (2021) Variables affecting shoot growth and plantlet recovery in tissue cultures of drug-type *Cannabis sativa* L. *Front Plant Sci*. <https://doi.org/10.3389/fpls.2021.732344>
- Jiang K, Asami T (2018) Chemical regulators of plant hormones and their applications in basic research and agriculture*. *Biosci Biotechnol Biochem* 82:1265–1300. <https://doi.org/10.1080/09168451.2018.1462693>
- Kepinski S, Leyser O (2005) The *Arabidopsis* F-box protein TIR1 is an auxin receptor. *Nature* 435:446–451. <https://doi.org/10.1038/nature03542>
- Klos D, Dušek M, Samol'ová E et al (2022) New water-soluble cytokinin derivatives and their beneficial impact on barley yield and photosynthesis. *J Agric Food Chem* 70:7288–7301. <https://doi.org/10.1021/acs.jafc.2c00981>
- Koprna R, De Diego N, Dundálková L, Spíchal L (2016) Use of cytokinins as agrochemicals. *Bioorg Med Chem* 24:484–492. <https://doi.org/10.1016/j.bmc.2015.12.022>
- Kurepa J, Smalle JA (2022) Auxin/Cytokinin Antagonistic Control of the Shoot/Root Growth Ratio and Its Relevance for Adaptation to Drought and Nutrient Deficiency Stresses. *Int J Mol Sci* 23:1933. <https://doi.org/10.3390/ijms23041933>
- Lata H, Chandra S, Khan I, ElSohly MA (2009) Thidiazuron-induced high-frequency direct shoot organogenesis of *Cannabis sativa* L. *Vitr Cell Dev Biol - Plant* 45:12–19. <https://doi.org/10.1007/s11627-008-9167-5>
- Lata H, Chandra S, Techen N et al (2016) In vitro mass propagation of *Cannabis sativa* L.: A protocol refinement using novel aromatic cytokinin meta-topolin and the assessment of eco-physiological, biochemical and genetic fidelity of micropropagated plants. *J Appl Res Med Aromat Plants* 3:18–26. <https://doi.org/10.1016/j.jarmap.2015.12.001>
- Lee S, Sundaram S, Armitage L et al (2014) Defining binding efficiency and specificity of auxins for SCF^{TIR1}/AFB-Aux/IAA Co-receptor complex formation. *ACS Chem Biol*. <https://doi.org/10.1021/cb400618m>
- Liang Y, Jiang C, Liu Y et al (2020) Auxin regulates sucrose transport to repress petal abscission in rose (*Rosa hybrida*). *Plant Cell* 32:3485–3499. <https://doi.org/10.1105/tpc.19.00695>
- Lin W, Zhou X, Tang W et al (2021) TMK-based cell-surface auxin signalling activates cell-wall acidification. *Nature* 599:278–282. <https://doi.org/10.1038/s41586-021-03976-4>
- Ma L, Li G, Li S, Jiang S (2020) An improved protocol for whole mount clearing of plant root tip. *Chinese Bull Bot* 55:596–604
- Mansouri H, Bagheri M (2017) Induction of Polyploidy and Its Effect on *Cannabis sativa* L. In: *Cannabis sativa* L. - Botany and Biotechnology. Springer International Publishing, Cham, pp 365–383
- Marc J, Granger CL, Brincat J et al (1998) A GFP–MAP4 reporter gene for visualizing cortical microtubule rearrangements in living epidermal cells. *Plant Cell* 10:1927–1939. <https://doi.org/10.1105/tpc.10.11.1927>
- Monthony AS, Kyne ST, Grainger CM, Jones AMP (2021a) Recalcitrance of *Cannabis sativa* to de novo regeneration; a multi-genotype replication study. *PLoS ONE* 16:1–17. <https://doi.org/10.1371/journal.pone.0235525>
- Monthony AS, Page SR, Hesami M, Jones AMP (2021b) The past, present and future of *cannabis sativa* tissue culture. *Plants* 10:1–29. <https://doi.org/10.3390/plants10010185>
- Movahedi M, Ghasemiomran V, Torabi S (2016) Effect of explants type and plant growth regulators on in vitro callus induction and shoot regeneration of *Cannabis sativa* L. Iran. *J Med Aromat Plants Res* 32:83–97
- Murashige T, Skoog F (1962) A revised medium for rapid growth and bio assays with tobacco tissue cultures. *Physiol Plant* 15:473–497. <https://doi.org/10.1111/j.1399-3054.1962.tb08052.x>
- Oono Y, Ooura C, Rahman A et al (2003) p-chlorophenoxyisobutyric acid impairs auxin response in *Arabidopsis* root. *Plant Physiol* 133:1135–1147. <https://doi.org/10.1104/pp.103.027847>
- Piunno KF, Golenia G, Boudko EA et al (2019) Regeneration of shoots from immature and mature inflorescences of *Cannabis sativa*. *Can J Plant Sci* 99:556–559. <https://doi.org/10.1139/cjps-2018-0308>
- R Core Team (2022) R: A language and environment for statistical computing. R Foundation for Statistical Computing, Vienna, Austria. <https://www.R-project.org/>
- Rademacher W (2015) Plant Growth Regulators: Backgrounds and Uses in Plant Production. *J Plant Growth Regul* 34:845–872. <https://doi.org/10.1007/s00344-015-9541-6>
- Razmienė B, Řezníčková E, Dambrauskienė V et al (2021) Synthesis and Antiproliferative Activity of 2,4,6,7-Tetrasubstituted-2H-pyrazolo[4,3-c]pyridines. *Molecules* 26:6747. <https://doi.org/10.3390/molecules26216747>
- Rigal A, Ma Q, Robert S (2014) Unraveling plant hormone signaling through the use of small molecules. *Front Plant Sci*. <https://doi.org/10.3389/fpls.2014.00373>
- Sayed GH, Elhalim MSA (1981) Nucleophilic-addition of indoles to beta-aroilacrylic acids and some reactions with the adducts. *Indian J Chem Sect B-Organic Chem Incl Med Chem* 20:424–426
- Schriever C, Lamshoef M (2020) Lipophilicity matters: a new look at experimental plant uptake data from literature. *Sci Total Environ*. <https://doi.org/10.1016/j.scitotenv.2020.136667>
- Shi H, Chen L, Ye T et al (2014) Modulation of auxin content in *Arabidopsis* confers improved drought stress resistance. *Plant Physiol Biochem* 82:209–217. <https://doi.org/10.1016/j.plaphy.2014.06.008>
- Skalák J, Vercauysen L, Claeys H et al (2019) Multifaceted activity of cytokinin in leaf development shapes its size and structure in *Arabidopsis*. *Plant J*. <https://doi.org/10.1111/tpj.14285>
- Smýkalová I, Vrbová M, Cvečková M et al (2019) The effects of novel synthetic cytokinin derivatives and endogenous cytokinins on the in vitro growth responses of hemp (*Cannabis sativa* L.) explants. *Plant Cell Tissue Organ Cult* 139:381–394. <https://doi.org/10.1007/s11240-019-01693-5>
- Tamaki H, Reguera M, Abdel-Tawab YM et al (2015) Targeting hormone-related pathways to improve grain yield in rice: a chemical approach. *PLoS ONE*. <https://doi.org/10.1371/journal.pone.0131213>
- Torii KU, Hagihara S, Uchida N, Takahashi K (2018) Harnessing synthetic chemistry to probe and hijack auxin signaling. *New Phytol* 220:417–424. <https://doi.org/10.1111/nph.15337>
- Uchida N, Takahashi K, Iwasaki R et al (2018) Chemical hijacking of auxin signaling with an engineered auxin–TIR1 pair. *Nat Chem Biol* 14:299–305. <https://doi.org/10.1038/nchembio.2555>
- Ulmasov T, Hagen G, Guilfoyle TJ (1997) ARF1, a transcription factor that binds to auxin response elements. *Science*. <https://doi.org/10.1126/science.276.5320.1865>

- Umehara M, Hanada A, Yoshida S et al (2008) Inhibition of shoot branching by new terpenoid plant hormones. *Nature* 455:195–200. <https://doi.org/10.1038/nature07272>
- Vain T, Raggi S, Ferro N et al (2019) Selective auxin agonists induce specific AUX/IAA protein degradation to modulate plant development. *Proc Natl Acad Sci U S A* 116:6463–6472. <https://doi.org/10.1073/pnas.1809037116>
- Villalobos L, Lee S, De Oliveira C et al (2012) A combinatorial TIR1/AFB-Aux/IAA co-receptor system for differential sensing of auxin. *Nat Chem Biol* 8:477–485. <https://doi.org/10.1038/nchembio.926>
- Zhang Q, Lin F, Mao T et al (2012) Phosphatidic acid regulates microtubule organization by interacting with MAP65-1 in response to salt stress in Arabidopsis. *Plant Cell* 24:4555–4576. <https://doi.org/10.1105/tpc.112.104182>
- Zhang C, Žukauskaitė A, Petřík I et al (2021) In situ characterisation of phytohormones from wounded Arabidopsis leaves using desorption electrospray ionisation mass spectrometry imaging. *Analyst* 146:2653–2663. <https://doi.org/10.1039/D0AN02118K>

Publisher's Note Springer Nature remains neutral with regard to jurisdictional claims in published maps and institutional affiliations.

Authors and Affiliations

Asta Žukauskaitė¹  · Iñigo Saiz-Fernández² · Kristýna Bielešzová¹ · Monika Iškauskienė³ · Chao Zhang⁴ · Iva Smýkalová⁵ · Karolína Dzedulionytė³ · Martin F. Kubes^{4,6} · Michaela Sedlářová⁷ · Barbora Pařízková⁴ · Iva Pavlovič⁴ · Thomas Vain^{8,9} · Ivan Petřík⁴ · Vida Malinauskienė³ · Algirdas Šačkus³ · Miroslav Strnad⁴ · Stéphanie Robert⁸ · Richard Napier⁶ · Ondřej Novák⁴ · Karel Doležal^{1,4}

✉ Asta Žukauskaitė
asta.zukauskaite@upol.cz

✉ Karel Doležal
karel.dolezal@upol.cz

- ¹ Department of Chemical Biology, Faculty of Science, Palacký University, Šlechtitelů 27, 78371 Olomouc, Czech Republic
- ² Department of Molecular Biology and Radiobiology, Faculty of AgriSciences, Phytophthora Research Centre, Mendel University in Brno, Zemědělská 1, 61300 Brno, Czech Republic
- ³ Department of Organic Chemistry, Faculty of Chemical Technology, Kaunas University of Technology, Radvilėnu Pl. 19, 50254 Kaunas, Lithuania

⁴ Laboratory of Growth Regulators, Palacký University and Institute of Experimental Botany of the Czech Academy of Sciences, Šlechtitelů 27, 78371 Olomouc, Czech Republic

⁵ Agritec Plant Research s.r.o., Zemědělská 2520/16, 78701 Šumperk, Czech Republic

⁶ School of Life Sciences, University of Warwick, Coventry CV47AL, UK

⁷ Department of Botany, Faculty of Science, Palacký University, Šlechtitelů 27, 78371 Olomouc, Czech Republic

⁸ Department of Forest Genetics and Plant Physiology, Umeå Plant Science Centre, Swedish University of Agricultural Sciences, 90183 Umeå, Sweden

⁹ Present Address: Technical University of Denmark, Centrifugevej 374, 2800 Kgs. Lyngby, Denmark